XVI International Symposium on Very High Energy Cosmic Ray Interactions
ISVHECRI 2010, Batavia, IL, USA (28 June 2 July 2010)

1

Phenomenological Approach to Multiple Particle Production

— A model to describe (pseudo-)rapidity density distributions and transverse momentum distributions in a wide energy region —

A. Ohsawa

Institute for Cosmic Ray Research, University of Tokyo, Kashiwa, 277-8582 Japan.

E.H. Shibuya

Instituto de Fisica Gleb Wataghin, Universidade Estadual de Campinas, Campinas, 13083-970 Brasil.

M. Tamada

School of Science and Engineering, Kinki University, Higashi-Osaka, 577-8502 Japan.

We formulate empirically the rapidity density distribution of produced particles in multiple particle production. The assumed mechanism is that the produced particles are emitted isotropically from several emitting centers, located on the rapidity axis. The formula includes five adjustable parameters, which are to be determined by the experimental data of (pseudo-)rapidity density distributions and transverse momentum distributions at various energies. It is a distinguished difference of the present rapidity density distribution from those of other models that the particle production is suppressed strongly in the forward region. We discuss multiplicity and inelasticity at high energies, the pseudo-rapidity density distribution at LHC energy and some speculations, based on the present formulation.

1. Introduction

We formulate the rapidity density distribution of produced particles *phenomenologically* and *analytically* on the basis of simple assumptions. It may clarify what kinds of mechanism are necessary essentially to describe multiple particle production and provide a model which can be extrapolated with more confidence[1] into higher energies.

2. Assumptions and formulae

2.1. Assumed mechanism of multiple particle production

We assume the following for the mechanism of multiple particle production.

(1) Produced particles are emitted isotropically from several emitting centers, which are distributed on the rapidity axis. (Fig. 1)

(2) Produced particles are the *newly* produced ones excluding the surviving particle. We assume that all produced particles are pions (mass m) tentatively. (An effect of kaons among the produced particles is not large for the (pseudo-)rapidity density distribution.[1])

---

[1] We have to say that most of the models of multiple particle production, proposed so far, do not reproduce even the basic data of multiple particle production reasonably, when we examine them in a wide range of energy. It means that the models include some inadequate points in them. We cannot put confidence on the properties of multiple particle production at high energies which are obtained by extrapolating such models.
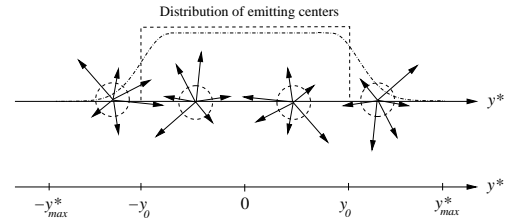
Figure 1: Produced particles are emitted isotropically from several emitting centers, located on the rapidity axis y^* in CMS (the center of mass system). The distribution of emitting centers is a simple flat one of eq.(2) (the chain line). The Fermi distribution of eq.(3) (the chain-dot line) is shown together for comparison. $y^*_{max} = \ln(\sqrt{s}/M)$ ($\sqrt{s}$: the energy in CMS, M : nucleon mass) and $y_0 = y^*_{max} - \ln a_2$ (a_2 : an adjustable parameter).

(3) The normalized energy distribution of produced particles in the rest frames of respective emitting centers is

$$f(p)dp = \frac{p^2}{2(1+r)} \left[\frac{1}{p_1^3} e^{-p/p_1} + \frac{r}{p_2^3} e^{-p/p_2} \right] dp \quad (1)$$

where the values of the parameters p_1 and p_2 ($p_1 < p_2$) are determined so as to reproduce the p_T (transverse momentum) distributions at $\sqrt{s} = 63$, 546 and 1800 GeV. That is, the first and the second term in the energy distribution correspond to the p_T distributions in the low and high p_T region, respectively. (We showed in Ref.[1] that the p_T distribution cannot be described by a single exponential function of the energy distribution.) The parameter r is the relative contribution of the second term. (The term p^2 is necessary to reproduce the p_T distribution in the vicinity of $p_T = 0$.)

(4) The distribution of the emitting centers in CMS

XVI International Symposium on Very High Energy Cosmic Ray Interactions
ISVHECRI 2010, Batavia, IL, USA (28 June 2 July 2010)

2

(the center of mas system) is a "simple flat" one;

$$g(y')dy' = \frac{dy'}{y_0} \quad (0 \leq y' \leq y_0) \quad (2)$$

where $y_0 = y_{max}^* - \ln a_2$ and $y_{max}^* = \ln(\sqrt{s}/M)$ ($\sqrt{s}$: the CMS energy, M : nucleon mass).[2] (see Fig. 1)

The parameter a_2 describes shrinkage of the (pseudo-)rapidity density distribution in the forward region, and the value of it is determined so as to reproduce (pseudo-)rapidity density distributions in the region-3[3] at various energies. Note that the distribution is normalized to one in the forward hemisphere.

We examined another type of the emitting center distribution,

$$g(y')dy' = \frac{c}{1 + e^{b(y'-y_0)}}dy' \quad (3)$$

with $b = 2.0$ and $c = b/\ln(1 + e^{by_0})$, which will be called "Fermi distribution". (see Fig. 1)

2.2. Rapidity density distribution

The normalized energy-angular distribution of a produced particles in the rest frame of an emitting center is

$$f(p)dp\frac{1}{2}d(\cos\theta)$$

where the variable θ is the zenith angle of the produced particle in the rest frames of respective emitting centers. By the variable transformation it turns to

$$\frac{p_T E}{2p^2}dydp_T$$

where the variable y is the rapidity in the rest frames of respective emitting centers. Since the rapidity of a produced particle in CMS is $y^* = y' + y$, the rapidity density distribution of charged produced particles in CMS is

$$\frac{d^2 N_{ch}}{dy^* dp_T} = a_1 y_0 \int_{-\infty}^{\infty} \frac{p_T E}{2p^2} f(p)g(y')dy'$$

$$= a_1 \int_{-y_0}^{y_0} dy' \frac{p_T E}{2(r+1)} \left[\frac{1}{p_1^3}e^{-p/p_1} + \frac{r}{p_2^3}e^{-p/p_2} \right] \quad (4)$$

---

[2]The quantities with an asterisk are those in CMS.

[3]We divide the rapidity region between $y^* = 0$ and $y^* = y_{max}^* = \ln(\sqrt{s}/M)$ roughly into three regions, region-1, -2 and -3. The rapidity density is flat in the region-1, decreasing gradually in the region-2 and is small, for example, less than a half of the density at $y^* = 0$, in the region-3. The pseudo-rapidity region is divided similarly, too.

where $E = \mu\cosh(y^* - y')$, $p = \sqrt{E^2 - m^2}$ and $\mu = \sqrt{p_T^2 + m^2}$. The parameter a_1 is related to the (pseudo-)rapidity density at $y^* = 0$, and the value of it is determined so as to reproduce the data at various energies. Note that the proportional coefficient is not a_1 but $a_1 y_0$ in eq.(4).

2.3. Pseudo-rapidity density distribution and x-distribution

The pseudo-rapidity density distribution and x-distribution (defined as $x^* = 2p_{||}^*/\sqrt{s}$, $p_{||}^*$: longitudinal momentum of produced particle in CMS) are obtained by variable transformations from eq.(4).

$$\frac{d^2 N_{ch}}{d\eta^* dp_T} = \frac{p_T(e^{\eta^*} + e^{-\eta^*})}{\sqrt{p_T^2(e^{\eta^*} + e^{-\eta^*})^2 + 4m^2}}\frac{d^2 N_{ch}}{dy* dp_T} \quad (5)$$

where

$$y^* = \ln \frac{p_T(e^{\eta^*} - e^{-\eta^*}) + \sqrt{p_T^2(e^{\eta^*} - e^{-\eta^*})^2 + 4\mu^2}}{2\mu}$$

$$\frac{d^2 N_{ch}}{dx^* dp_T} = \frac{1}{\sqrt{(x^*)^2 + (2\mu/\sqrt{s})^2}}\frac{d^2 N_{ch}}{dy^* dp_T} \quad (6)$$

where

$$y^* = \ln \frac{\sqrt{(x^*)^2 + (2\mu/\sqrt{s})^2} + x^*}{2\mu/\sqrt{s}}$$

2.4. p_T distribution

The p_T distribution (at $\theta^* = 90°$) in terms of the invariant cross section is

$$E\frac{d^3\sigma}{d^3p}\bigg|_{\theta=90°} = \frac{\sigma_{inel}}{2\pi p_T}\left(\frac{d^2 N_{ch}}{dy^* dp_T}\right)_{y^*=0} \quad (7)$$

The suffix $\theta = 90°$ will be omitted hereafter.

The local p_T average at the rapidity y^* is defined as

$$<p_T>_{y^*} = \int_0^\infty p_T \frac{d^2 N_{ch}}{dy^* dp_T}dp_T \bigg/ \int_0^\infty \frac{d^2 N_{ch}}{dy^* dp_T}dp_T \quad (8)$$

The local p_T average at the pseudo-rapidity η^*, $<p_T>_{\eta^*}$, is defined similarly, which is not the same as eq.(8) in general.

Note that the p_T average, obtained by the experiments, is either $<p_T>_{y^*=0}$ or $<p_T>_{\eta^*=0}$ in most of the experiments.

XVI International Symposium on Very High Energy Cosmic Ray Interactions
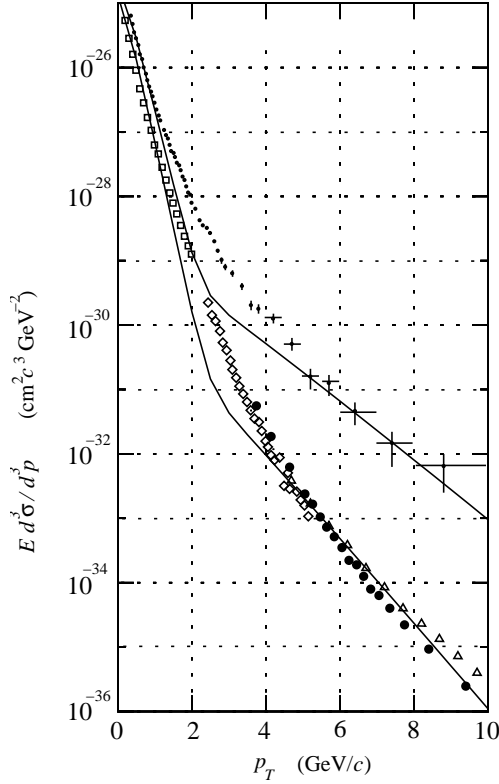*ISVHECRI 2010, Batavia, IL, USA (28 June 2 July 2010)*

3

Figure 2: The p_T distributions at $\sqrt{s} = 63$ GeV (the lower curve) and 546 GeV (the upper). Experimental data are compiled by UA1 Collaboration.[2] dots $((h^+ + h^-)/2)$: UA1 Collaboration for a half of charged hadrons at $\sqrt{s} = 546$ GeV, squares $((h^+ + h^-)/2)$, diamonds (π^0), triangles (π^0) and circles $((h^+ + h^-)/2)$: ISR data at $\sqrt{s} = 63$ GeV. Note that value of the curve in the ordinate is a half of eq.(7) with the values of the parameters in Table 1.

2.5. Multiplicity and inelasticity

Since the distribution of the emitting centers is normalized in the forward hemisphere, charged multiplicity m_{ch} is twice of the normalization coefficient in eq.(4),

$$m_{ch} = 2a_1 y_0 = 2a_1 \left[\ln \left(\frac{\sqrt{s}}{M} \right) - \ln a_2 \right] \qquad (9)$$

The total inelasticity in CMS is

$$K = \frac{3}{2} \int_0^1 x^* \left(\frac{dN_{ch}}{dx^*} \right) dx^* \qquad (10)$$

3. Values of the parameters

3.1. Values of the parameters p_1, p_2 and r

The values of the parameters in the energy distribution of eq.(1) are determined by fitting the p_T
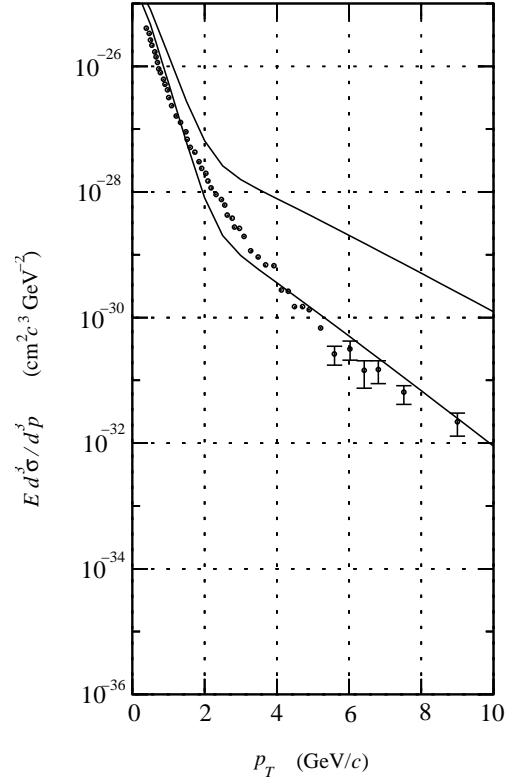
Figure 3: The p_T distributions at 1800 GeV (the lower curve) and 14 TeV (the upper). Experimental data are for a half of charged hadrons, $(h^+ + h^-)/2$, from CDF Collaboration.[3] Note that value of the curve in the ordinate is a half of eq.(7) with the values of the parameters in Table 1.

distribution of eq.(7) to those of the experiments at $\sqrt{s} = 63$, 546 and 1800 GeV,[2, 3] which are shown in Figs. 2 and 3.

Values of the parameters determined are tabulated in Table 1. The values of the parameters p_1 and p_2 are determined to reproduce the slopes of the p_T distributions in the p_T regions of $0.2 - 1.0$ and $5.0 - 10.0$ (GeV/c), respectively. The value of the parameter a_1 in Table 1 is determined by equating the calculated pseudo-rapidity density at $\eta^* = 0$ to that of the experiment.[4] (In the calculation we assume the value of the parameter $a_2 = 1.0$, which affects slightly the pseudo-rapidity density at $\eta^* = 0$.) One can see in the figures that the p_T distributions are described well in the small and large p_T regions, but not in the middle p_T region.

Fig. 4 shows the energy dependences of the parameters p_1, p_2 and r in Table 1. Assuming the power dependences of the energy, empirical formulae of the parameters are;

$$\begin{aligned} p_1 &= 0.0895(\sqrt{s})^{0.109} \\ p_2 &= 0.381(\sqrt{s})^{0.130} \\ r &= 2.38 \times 10^{-6}(\sqrt{s})^{1.07} \end{aligned} \qquad (11)$$

XVI International Symposium on Very High Energy Cosmic Ray Interactions
ISVHECRI 2010, Batavia, IL, USA (28 June 2 July 2010)

4

Table I Values of the parameters for the p_T distributions

$\sqrt{s}$ (GeV)	p_1 or p_2 (GeV/c)	$(dN_{ch}/d\eta^*)_{\eta^*=0}$ cal.	exp.	a_1	σ_{inel} (mb)	r	Ref.
63	$p_1 = 0.154$ $p_2 = 0.632$	$0.843a_1$	1.88 ± 0.08	2.23	36.0	2.0×10^{-4}	[2]
546	$p_1 = 0.1175$ $p_2 = 0.895$	$0.865a_1$	2.79 ± 0.08	3.23	49.0	2.0×10^{-3}	[2]
1800	$p_1 = 0.206$ $p_2 = 0.938$	$0.875a_1$	3.95^*	4.51	56.0	2.0×10^{-3}	[3]
1.4×10^4	$p_1 = 0.253$ $p_2 = 0.632$	–	–	6.54	$73.0^\dagger$	6.5×10^{-2}	

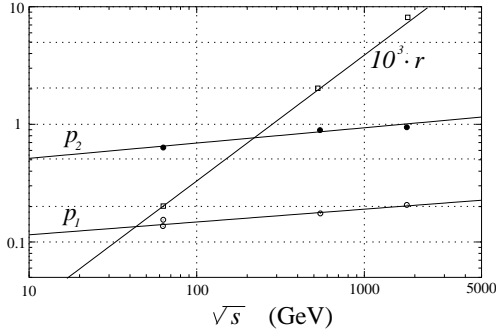* : the value at $\eta^* = 0.12$, $\quad ^\dagger$: Model 2 in Ref.[7]

Figure 4: Energy dependences of the parameters p_1 (GeV/c) (open circles), p_2 (GeV/c) (full circles) and r (squares). Note that the parameter r is multiplied by a factor 10^3. The solid lines are eq.(11), the best-fit ones to the data points, assuming the power dependences of the energy $\sqrt{s}$.

where the energy $\sqrt{s}$ is in GeV.

We expected that the parameters p_1 and p_2 are energy-independent, which is not correct. The value of the parameter r exceeds 1.0 for the energy $\sqrt{s} > 1.80 \times 10^5$ GeV, since the exponent is as large as 1.07. We can append, however, that the cross section of mini-jets ($E_T > 5$ GeV, $|\eta^*| < 1.5$) increases similarly in the energy region $\sqrt{s} = 200 - 900$ GeV.[5] We should note that the exponent may become smaller than 1.07 at high energies, since the channel of mini-jets has opened just in the present energy region.

Fig. 5 shows the p_T average at $\eta^* = 0$, $< p_T >_{\eta^*=0}$, and the energy $\sqrt{s}$, based on the energy dependences of the parameters in eq.(11). It is of no wonder that experimental data are consistent with that at $\eta^* = 0$ (but not at $y^* = 0$), since the condition to sample the events refers the pseudo-rapidity in the data concerned.

Fig. 6 shows the local p_T average at the rapidity y^* for various values of the parameter a_2, together with the data in the region-3. The data are from UA7 Collaboration at $\sqrt{s} = 630$ GeV.[6] The data are described well by the curve of $a_2 = 5.0$. It is important to note that the rapidity density distribution
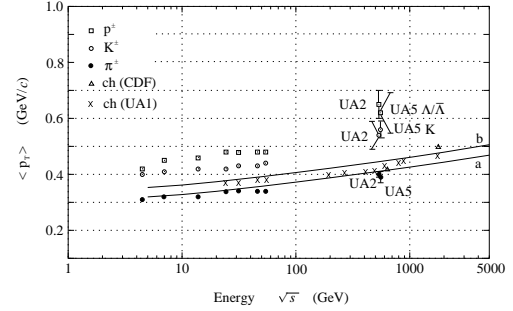

Figure 5: The p_T average and the energy $\sqrt{s}$. The data are those compiled by UA5 Collaboration[2] and by UA1 Collaboration[8] and those from CDF Collaboration.[3] The curves are $< p_T >_{y^*=0}$ (denoted as "a") and $< p_T >_{\eta^*=0}$ ("b"), which are defined in 2.4.
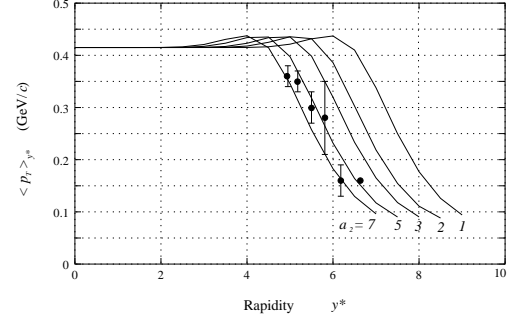

Figure 6: The local p_T average of eq.(8) at $\sqrt{s} = 630$ GeV. The curves are for the values of the parameter $a_2 = 1.0$, 2.0, 3.0, 5.0 and 7.0 (attached to the curves). Data are for π^0's by UA7 Collaboration.[6] The data are described well by the curve of $a_2 = 5.0$.

in the region-3, obtained by the same collaboration, is described by the same value of the parameter a_2 simultaneously. (see 3.2)

3.2. Values of the parameters a_1 and a_2

The values of the parameters a_1 and a_2 are determined by fitting the (pseudo-)rapidity density distri-

XVI International Symposium on Very High Energy Cosmic Ray Interactions
ISVHECRI 2010, Batavia, IL, USA (28 June 2 July 2010)

5

bution, eqs.(4) or (5), to those of experiments at various energies. Note that the surviving particle is included among the observed particles in most of the experimental data. The density of the surviving particle, however, occupies a small part of the (pseudo-) rapidity density in the region-1 and -2 where the data exist. (see, for example, Fig. 13)

Sources of the experimental data of the (pseudo-) rapidity density distribution are tabulated in Table 2. The data in the table concern only those that are necessary for the present analysis. For example, EHS-NA22 Collaboration observed $K^+ p$ and $\pi^+ p$ collisions, too. Necessary comments to respective sets of data are found in Ref.[1].

Figs. 7, 8 and 9 are the examples to show how well the experimental data are described by the curves of the present formulation. The curves are calculated for several assumed values of the parameters a_1 and a_2, *i.e.* $a_1 = 1.0$ and $a_2 = 1.0$, 2.0, $\cdots$. Hence, in the figures, the calculated curves are shifted upwards to fit to the data in the region-1, and then the curve, which fits best to the data in the region-2 and/or -3, is selected. This procedure determines the values of the parameters a_1 and a_2, which are tabulated in Table 2. (The value of the parameter a_2 cannot be determined for the data by CDF Collaboration, since the data exit only in the region-1.) We list some comments below to the figures.
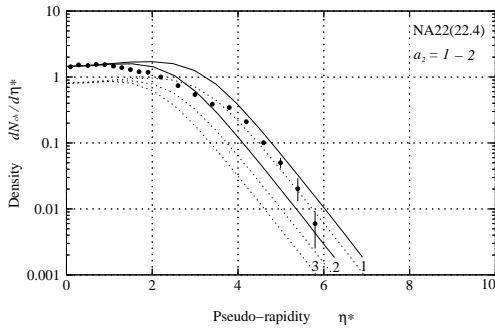

Figure 7: Pseudo-rapidity density distribution at $\sqrt{s} = 22.4$ GeV. The data are the sum of π^- (negative pions) and c^+ (positive particles) by EHS-NA22 Collaboration.[9] Dotted curves are eq.(5) with the values of the parameters $a_1 = 1.0$ and $a_2 = 1.0$, 2.0 and 3.0 (attached to the curve). The solid lines are the best-fit ones to the experimental data with the values of the parameters $a_1 = 1.8$ and $a_2 = 1.0 - 2.0$. Agreement between the curves and the data is poor in the region-2.

(1) In Fig. 7 the agreement between the best-fit curves and the data is good in the region-1 and -3, but is poor in the region-2. This situation is the same for almost all sets of data in Table 2. In Ref.[1] we showed that the Fermi distribution for the emitting centers, eq.(3), brings better agreement in the region-2, but that it does not describe the data of the local p_T average in the region-3, obtained by UA7 Collaboration.

One can see, however, in 3.1 that the simple flat distribution for the emitting centers describe the local p_T average naturally, which is the reason why we adopt it in the present paper.
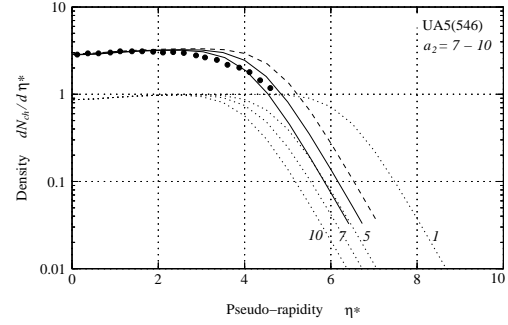

Figure 8: Pseudo-rapidity density distribution at $\sqrt{s} = 546$ GeV. Data are by UA5 Collaboration.[4] Dotted curves are eq.(5) with the values of the parameters $a_1 = 1.0$ and $a_2 = 1.0$, 5.0, 7.0 and 10.0 (attached to the curve). The solid lines are the best-fit ones to the experimental data with the values of the parameters $a_1 = 3.1$ and $a_2 = 7.0 - 10.0$. The chain line is for the values of the parameters $a_1 = 3.1$ and $a_2 = 5.0$, which corresponds approximately to the assumed case of the inelasticity $K = 0.5$. (see eq.(12)) Note that the chain curve *does not* describe the data clearly.

(2) Fig. 8 shows the pseudo-rapidity density distributions at $\sqrt{s} = 546$ GeV, together with the experimental data by UA5 Collaboration.[4] The curves of $a_1 = 3.1$ and $a_2 = 7$ and 10 describe the data reasonably.

(3) In Fig. 9 the value of the parameter $a_1 = 3.5$ for the data by UA7 Collaboration[6] is the assumed one, since data exist only in the region-3. It is important to note that the rapidity density distribution is described well by the value of the parameter $a_2 = 5.0$ which describes the local p_T average in Fig. 6.
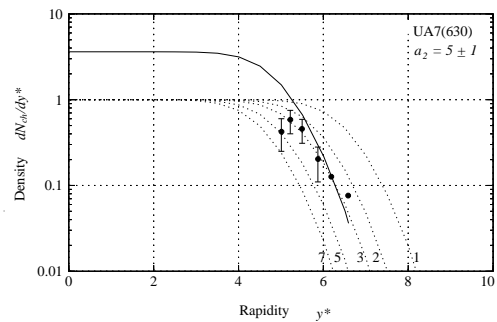

Figure 9: Rapidity density distribution at $\sqrt{s} = 630$ GeV. Data of π^0's, by UA7 Collaboration[6], are multiplied by a factor 2.0. Dotted lines are those for the values of the parameters $a_1 = 1.0$ and $a_2 = 1.0$, 2.0, 3.0, 5.0 and 7.0 (attached to the curves). The solid line is the best-fit one with the values of the parameters $a_1 = 3.5$ (assumed) and $a_2 = 5.0$.

Insert PSN Here

6

XVI International Symposium on Very High Energy Cosmic Ray Interactions
ISVHECRI 2010, Batavia, IL, USA (28 June – 2 July 2010)

Table II Data of (pseudo-)rapidity density distributions and the values of the parameters a_1 and a_2

Collab.	Site	Energy $\sqrt{s}$ (GeV)	Collision	Observed particles[†]	Observed range	Observed quantity	Parameter a_1	a_2	Ref.
EHS-NA22	CERN SPS	22.4	pp	π^-, c^+	$|\eta^*| \le 6.0$	$d\sigma/d\eta^*$	1.8	1.5 ± 0.5	[9]
Phobos	BNL RHIC	200	pp	$c^\pm$	$|\eta^*| \le 5.4$	$dN/d\eta^*$	2.6	4 ± 1	[10]
UA5	CERN SPS	53	$\bar{p}p$	$c^\pm$	$|\eta^*| \le 3.5$	$dN/d\eta^*$	2.1	3 ± 1	[4]
		200			$|\eta^*| \le 4.6$		2.6	4 ± 1	
		546			$|\eta^*| \le 4.6$		3.1	8.5 ± 1.5	
		900			$|\eta^*| \le 4.6$		3.5	10 ± 1	
UA7	CERN SPS	630	$\bar{p}p$	γ	$y^* = 5.0 - 6.6$	$d\sigma_{\pi^0}/dy^*$	(3.5)	5 ± 1	[6]
P238	CERN SPS	630	$\bar{p}p$	$c^\pm$	$\eta^* = 1.5 - 5.5$	$dN/d\eta^*$	3.5	6 ± 1	[11]
CDF	FNAL Tevatron	630	$\bar{p}p$	$c^\pm$	$|\eta^*| \le 3.5$	$dN/d\eta^*$	3.6	–	[12]
		1800					4.4	–	

[†] The letter c stands for charged particles.

Fig. 10 shows the energy dependences of the parameters a_1 and a_2 in Table 2. We list some comments to Fig. 10.

(1) Since the (pseudo-)rapidity density distribution is almost flat in the region-1, it is easy to fit the data to the calculated curve. Consequently the values of the parameter a_1 are determined reliably to reproduce the data.

(2) In the accelerator experiments it is not easy to obtain the data in the region-2 and -3 due to the experimental conditions. Consequently the data in the concerned regions are limited or missed in most of the experiments in Table 2, and the data in the region-2, if they exist, are often not consistent one another by the experiments even at the same incident energy. Consequently the values of the parameter a_2 are determined with large errors and are distributed widely.

(3) In order to consider the *assumed* case of the inelasticity $K = 0.5$, we examine the energy dependence of the parameter

$$a_2 = 0.718(\sqrt{s})^{0.320} \qquad (12)$$

As can be seen in Fig. 12, eq.(12) brings the inelasticity $K \simeq 0.5$, taking the value of the parameter a_1 as it is, one of eq.(13). In Fig. 10 the chain-dot line of eq.(12) is almost consistent with points except those at $\sqrt{s} = 546$ and 900 GeV, both of which are from UA5 Collaboration. (Fig. 8 shows that the pseudo-rapidity density distribution at $\sqrt{s} = 546$ GeV by UA5 Collaboration is not described by the curve of the assumed case of $K = 0.5$ clearly.) It is not evident, however, that both data are biased in the region-2 seriously. Since it is our strategy in the present paper to formulate multiple particle production phenomenologically avoiding *a priori* assumptions as much as possible, we determine the energy dependence of the parameter a_2 by the least square method including both data.
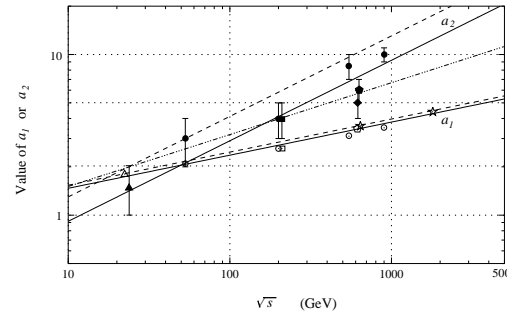
Assuming the power law for the energy dependences

Figure 10: The values of the parameters a_1 (open marks) and a_2 (full marks) in Table 2 and the energy $\sqrt{s}$. Marks: triangles (EHS-NA22 Collaboration), circles (UA5), squares (Phobos), pentagons (P238), diamonds (UA7), stars (CDF). Solid lines are the best-fit ones to the data points, eq.(13) in the text. Chain lines are those in Ref.[1]. The chain-dot line is eq.(12) in the text, for which the total inelasticity is $K = 0.5$.

of the parameters a_1 and a_2, we obtain ($\sqrt{s}$ in GeV)

$$\begin{aligned} a_1 &= 0.915(\sqrt{s})^{0.206} \\ a_2 &= 0.289(\sqrt{s})^{0.501} \end{aligned} \qquad (13)$$

which are shown in Fig. 10.

4. Discussions

(i) *Energy dependence of the multiplicity*

Fig. 11 shows the energy dependence of the charged multiplicity, eq.(9), by the present formulation, together with experimental data.[4] It describes the data well at high energies of $\sqrt{s} > 50$ GeV. The data at lower energies are described better by the curve of the assumed case of the inelasticity $K = 0.5$. (see the text below for the value of the inelasticity at low energies)
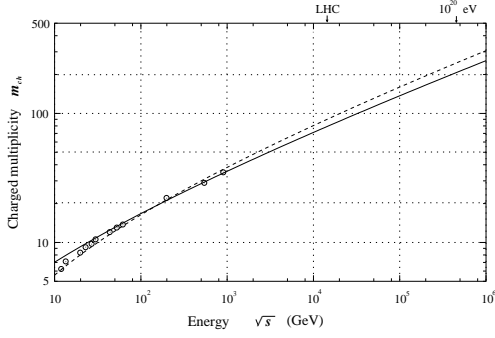
Figure 11: Energy dependence of the charged multiplicity m_{ch}, defined by eq.(9). The solid line is for the values of the parameters in eq.(13). Experimental data are compiled by UA5 Collaboration.[4] The chain line is for the assumed case of eq.(12), for which the inelasticity remains constant (~ 0.5).
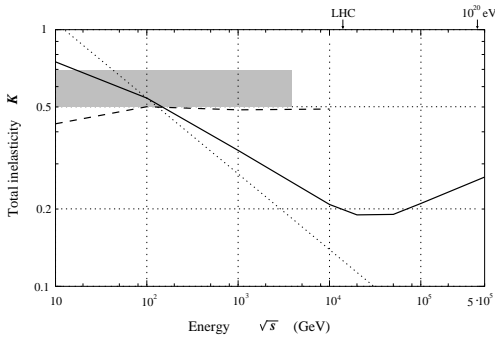

Figure 12: Energy dependence of the total inelasticity, defined by eq.(10), by the present formulation. (the solid line) The inelasticity decreases with the energy in the energy region $\sqrt{s} < 2 \times 10^4$ GeV, and then increases.

The shaded area is the predictions by some models of multiple particle production.[13] Note that the predicted quantities are not exact inelasticities but $(1 - \eta')$'s where the parameter η' is the energy fraction of the highest energy baryon among the produced particles. ("Produced particles" here include the surviving particle, which is different from the definition in the present paper.)

The dotted line is $a_1/a_2 \propto (\sqrt{s})^{-0.295}$, which is steeper than the inelasticity due to the energy dependence of the parameters p_1 and p_2 in the energy distribution. The chain line is for the assumed case of eq.(12), for which the inelasticity remains almost constant (~ 0.5).

(ii) *Energy dependence of the inelasticity*

Fig. 12 shows the energy dependence of the total inelasticity, eq.(10), by the present formulation. The inelasticity decreases with the energy in the energy region $\sqrt{s} < 2 \times 10^4$ GeV, due to the rapid increase of the parameter a_2, compared with the parameter a_1. (The inelasticity is proportional to a_1/a_2 approximately.) After that it increases, due to the exchange of the dominant parameter in the energy distribution from p_1 to p_2 ($p_1 < p_2$) through rapid increase of parameter r. (Experimental data of the inelasticity

Insert PSN Here

is $K \simeq 0.5$ at low energies around $\sqrt{s} = 10$ GeV by bubble chamber experiments.)

(iii) *Pseudo-rapidity density distribution at LHC energy*

Fig. 13 shows the pseudo-rapidity density distribution of the produced particles at $\sqrt{s} = 14$ TeV (LHC energy) by the present formulation. Compared with the predictions by other models, the shrinkage of the forward region is distinguished, which results in a small inelasticity of the present formulation. Predictions by the models are distributed widely, and even a single data of the pseudo-rapidity density at $\eta^* = 0$ can discriminate some models as improbable if they cannot modify their predictions.[4]

The distribution of the surviving particle is shown together in Fig.13. We assume that the charge exchange probability of the incident proton into neutrons is 0.5, details of which are described in Ref.[1].
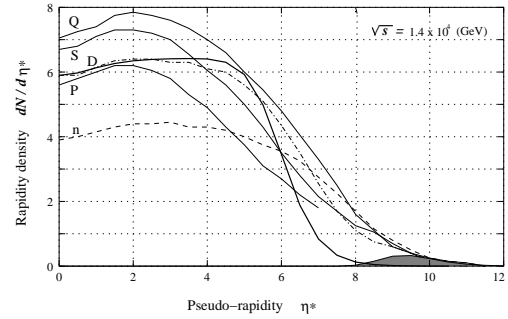

Figure 13: Pseudo-rapidity density distribution of produced particles (the solid line) and the surviving particle (the shaded area) at $\sqrt{s} = 14$ TeV (LHC energy). The thin lines are the predictions of the pseudo-rapidity density by some models.[14,15]
Q : QGSJET01, S : SIBYLL2.1, D : DPMJET2.55, P : PYTHIA, n : neXus2.1

(iv) *Speculations related to the inelasticity to decrease and to increase*

According to the present formulation the inelasticity is decreasing in the energy region $\sqrt{s} < 2 \times 10^4$ GeV ($E_0 < 2 \times 10^{17}$ eV) and then increasing in $\sqrt{s} > 5 \times 10^4$ GeV ($E_0 > 10^{18}$ eV). This structure of the inelasticity is caused by the rapid increase of the parameter a_2, compared with that of a_1, which means that particle production is suppressed strongly in the forward region.

The inelasticity is related to the attenuation mean free path of cosmic rays, which is a dominant factor to govern the cosmic-ray propagation in the atmosphere.

---

[4]It is not self-evident that the model, tuned at LHC energy, reproduces the low-energy data which are referred to tune it previously.

8

XVI International Symposium on Very High Energy Cosmic Ray Interactions
ISVHECRI 2010, Batavia, IL, USA (28 June 2 July 2010)

Small (Large) inelasticity makes the attenuation mean free path long (short). Consequently the development, rise and fall, of the air showers becomes slow (rapid), and the air shower size at the maximum development is small (large) since the total track length of the air shower particles is conserved. Hence there is a possibility that following problems may be cleared by the decreasing and increasing inelasticity.

(1) Intensity of the primary cosmic rays.

There is a discrepancy between the primary cosmic-ray intensities by balloon experiments of direct observation and by air shower experiments of indirect observation, the former being lower than the latter by a factor 2.[16]

(2) $< X_{max} >$ and $RMS(X_{max})$ by Auger Collaboration

According to Pierre Auger Collaboration to observe highest energy air showers, both the depth of shower maximum, $< X_{max} >$, and the dispersion of the maximum depth, $RMS(X_{max})$, are reaching the expected lines of the iron primaries from those of the proton primaries in the region $E_0 = 10^{18} - 4 \times 10^{19}$ eV.[17]

Detailed and quantitative discussions will be made elsewhere.

References

[1] A. Ohsawa, E.H. Shibuya and M. Tamada, J. Phys. **G37** (2010) 075003.

[2] G. Arnison et al., Phys. Lett. **118B** (1982) 173.

[3] F. Abe et al., Phys. Rev. Lett. **61** (1988) 1819.

[4] J.G. Alner et al., Phys. Rep. **154** Nos.5 & 6 (1987) 247.

[5] W. Scott, Proc. XXIII Intern. Conf. on High Energy Phys., ed. S. Loken (World Sci., 1987).

[6] E. Pare et al., Phys. Lett. **B242** (1990) 531.

[7] J. Hörandel, J. Phys. G **29** (2003) 2439.

[8] C. Albajar et al., Nucl. Phys. **B335** (1990) 261.

[9] M. Adamus et al., Z. Phys. **C39** (1988) 311.

[10] B.B. Back et al., J. Phys. **G30** (2004) S1133.

[11] R. Haar et al., Phys. Lett. **B401** (1997) 176.

[12] F. Abe et al., Phys. Rev. **D41** (1990) 2330.

[13] J. Knapp, D. Heck and G. Schatz, Preprint FZKA5828, Forschungszentrum Karlsruhe (1996).

[14] D. Heck, M. Risse and J. Knapp, Nucl. Phys. B (Proc. Suppl.) 122 (2003) 364.

[15] J-P. Revol, Nucl. Phys. B (Proc. Suppl.) 177-178 (2008) 60.

[16] J.R. Hörandel, Adv. Space Res., 41 (2008) 442.

[17] J. Abraham et al., Phys. Rev. Lett. **104**, 091101, (2010).